

Generating temperature cycle profiles of different solar photovoltaic module technologies from in-situ conditions for accurate prediction of thermomechanical degradation

Bebeto Nii Sampa Sampah*, Frank K. A. Nyarko, Benjamin Atribawuni Asaaga, Jefferson Aggor

Department of Mechanical Engineering, College of Engineering, Kwame Nkrumah University of Science and Technology Kumasi, GHANA

*Corresponding author: Email: bebetosampahns@gmail.com

Abstract – The IEC61215 TC200 is a rigorous approval thermal cycling test process that assesses the reliability of solar photovoltaic modules and offers a 25-year lifetime guarantee. However, previous research has shown that installed solar photovoltaic modules experience different rates of degradation depending on the location and climate with most research focused on crystalline silicon. In this study, outdoor weathering data obtained from a rig set up in Kumasi, Ghana for the year 2014, is used to generate thermal cycles for 5 different technologies including monocrystalline, polycrystalline, and amorphous silicon, Copper Indium Gallium Selenide (CIGS) and Heterojunction-With-Intrinsic-Thin-Layer (HIT). From the results, the highest yearly average of the maximum and minimum temperatures, and ramp rates of 54.8°C, 26.1°C, and 6.05°C/h respectively are recorded in CIGS. Polycrystalline recorded the least temperatures of 45.2°C and 23.9°C while HIT recorded the least ramp rate of 4.45°C/h. A comparison between the 2014 and the IEC61215 thermal cycles show extremely wide differences which could explain the higher degradation rates and shorter life of installed solar photovoltaic modules. The procedure adopted in this research can be repeated at different locations to obtain technology-specific thermal cycling profiles to evaluate the thermomechanical damage and predict the life of different solar photovoltaic modules.

Keywords: Temperature cycling, Ramp rates, Temperature gradient, Dwell time, IEC 61215/61416, Co-efficient of Thermal Expansion (CTE), in-situ data generation.

Received: 12/09/2022 – Revised 29/11/2022 – Accepted: 05/12/2022

I. Introduction

The commercial viability of PV systems is strongly dependent on the field performance, cost, and life. It is imperative for engineers to study and minimize degradation and failure modes exposed to PV systems during their operational lifetime to improve commercial viability [1]. PV modules are expected to function at 90% power capacity for the first 10 years of operation and 80% power capacity after 25 years [2]. However, these estimations are not guaranteed due to the various external

stresses PV modules are exposed to during field operation. These include temperature changes, moisture, humidity, mechanical stress, and irradiance [3].

One of the common failure modes in solar modules is thermo-mechanical fatigue. Solder joints are the most susceptible layers to thermal damage and contribute to 40.7% of failures reported in field operations. This can result from exposure to high temperatures during the soldering process at manufacturing. Also, the difference in the coefficient of thermal expansion induces expansion

and contraction in the various layers of solar modules at different rates during day and night temperature changes. The growth of intermetallic compounds (IMC) in the solder joints also contributes to thermomechanical damage [4].

To study reliability in PV modules, the choice of thermal cycling is an important factor. It is characterized by temperature fluctuations between peak day temperatures and low night temperatures, ramp rates, and dwell times [5]. Many researchers have resorted to the use of the IEC 61215/IEC 61646 TC 200 thermal cycles to study thermochemical damage [4, 6, 7]. The IEC 61215/IEC 61646 involves subjecting solar modules to temperatures ranging between $-40\text{ }^{\circ}\text{C}$ to $+85\text{ }^{\circ}\text{C}$, with ramp rates of $100\text{ }^{\circ}\text{C/h}$ and 10-minute dwells [8]. It is most commonly seen with researchers varying parameters of the TC 200 in the course of their research. This includes an increased number of cycles, higher temperature gradients, ramp rates, and dwell times [4, 6, 7]. However, these conditions do not properly define the thermal conditions that the solar modules are exposed to during field operation, which varies from place to place.

On the other hand, the use of field data to study degradation in PV modules is essential to generating more accurate results since their actual lifetime are climate and location dependent [3]. Cuddalorepatta et al. [9] reported the use of field conditions between the temperature ranges of $17\text{ }^{\circ}\text{C}$ to $63\text{ }^{\circ}\text{C}$ in their study on the durability of lead-free solder in crystalline silicon solar modules. One study used data obtained from two days of weather exposure in Doha, Qatar to represent a summer day and a winter day in the study of the reliability of PV modules [10].

There are different types of solar modules with a wide range of efficiencies, which depends on the types of semiconductor that were adopted during manufacture [11]. These include mono-crystalline silicon, polycrystalline silicon, microcrystalline silicon, copper indium selenide, cadmium telluride, amorphous silicon, gallium arsenide, and HIT solar modules [2, 12]. The most commonly used solar module is monocrystalline silicon, which dominates the market by 85%. This supports the fact that the majority of research carried out on solar module reliability involved monocrystalline silicon [10, 13, 14]. Some researchers adopted polycrystalline in their studies on thermomechanical reliability [4, 15]. A research used four different solar modules which include monocrystalline silicon, multicrystalline silicon, amorphous silicon, and CIGS solar modules to study the performances in the field [16]. The study also used data obtained from three consecutive days in Malaysia. From the literature, it can be seen that

there is limited use of field data in studies on solar module reliability. Moreover, most of this research is focused on crystalline silicon solar modules and an even lesser number on thin films. There is also limited research on the inclusion of different technologies in one test site.

The purpose of this study is to generate an in-situ thermal cycle profile for five (5) different solar PV module technologies in Kumasi, Ghana. This involves the use of data obtained in the year 2014 for solar modules including monocrystalline silicon, polycrystalline silicon, CIGS, amorphous silicon, and HIT to develop temperature profile cycles and subsequently generate five different thermal cycles to represent the different technologies at the test site.

II. Material and method

This study makes use of secondary data that was obtained from an outdoor climate monitoring rig. Figure 1(a) shows a number of solar photovoltaic modules that make up the rig. It involves monocrystalline silicon, polycrystalline silicon, CIGS, amorphous silicon, and HIT solar photovoltaic modules. Figure 1(b) shows the data collection substation. The list of solar photovoltaic module specifications and capacities is shown in Table 1. The rig was installed in 2012 through the African Renewable Energy Access program financed by the World Bank under the project title: "Capacity Upgrading for West African Partners in Renewable Energy Education". The rig can be found at the College of Engineering KNUST, Kumasi, Ghana, West Africa. Its site location is latitude 64000 N and longitude 13700 W , 250m above sea level. They are mounted on a rooftop inclined at an angle of 5 degrees, facing southwards. The rigs are connected to the grid by a 4 kW SMA Sunny Boy DC-AC inverter (SB 3800). Using a Bluetooth ad-hoc connection, five inverters are connected and configured to communicate with a SMA Sunny WebBox, to log and transfer data from the various photovoltaic technologies to a server to be stored. Using the university network, an online monitoring system is established for the SMA Sunny portal created on the server. To measure the module temperatures, calibrated platinum sensors with $\pm 0.5\text{ }^{\circ}\text{C}$ measurement accuracy, and $0.1\text{ }^{\circ}\text{C}$ resolution, placed on the backside center of each module are used. The data recorded by the system included environment temperature, module temperature, total insolation, operating current and voltage, wind speed, and total output power. The data captured starts in March 2012 and ends in May 2015. However, the point of focus

in this research was the year 2014 since it provided the greatest amount of data as compared to the other years.

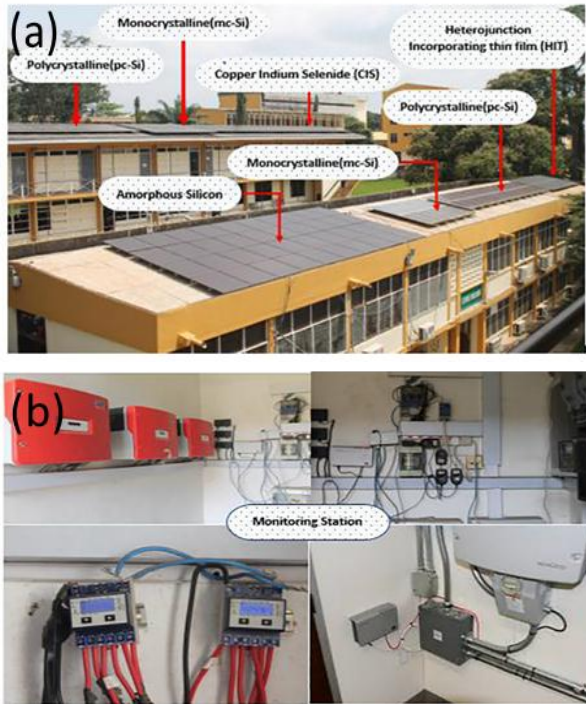


Figure 1. (a) Outdoor climate monitoring rig involving five different solar photovoltaic technologies. (b) Data collection substation [13].

Table 1. Solar photovoltaic module specifications and capacities.

Cell Technologies	Amorphous Silicon	Mono-crystalline Silicon	Poly-crystalline Silicon	HIT	CIGS
Model×String	10×4	7×3	9×2	8×2	9×9
Total number of modules	40	21	18	16	81
Power per module (W)	100	190	225	250	50
Total module peak power (W)	4000	3990	4050	4000	4050
Voltage at nominal power (V)	30.7	36.4	29.4	34.9	36.8
Current at nominal power (A)	3.25	5.22	7.55	7.18	1.36
Open circuit voltage (V)	40.9	45.2	36.7	43.1	49.5
Open circuit current (A)	3.85	5.46	8.24	7.74	1.66
Maximum system voltage (V)	1000	1000	1000	1000	1000
Temperature coefficient of open circuit voltage (%/°C)	-0.33	-0.33	-0.33	-0.01	-0.26
Temperature coefficient of short circuit current (%/°C)	0.08	0.03	0.04	0.03	0.04
Temperature coefficient Power (%/°C)	-0.2	-0.44	-0.45	-0.30	-0.30
Total surface area of PV system (m ²)	58.9	28.1	30.6	22.6	68.6
Nominal power of PV-module (kW)	4.0	3.99	4.05	4.0	4.05
Module efficiency (%)	6.9	14.5	13.7	18	6.1
NOCT	49	46	47.2	46	47

II.1. Generating Daily Temperature Profile

The 288 data points of module temperature recorded at intervals of 5 minutes were extracted for the various photovoltaic technologies according to their days. The module temperature columns for the various technologies were extracted and arranged by days of the month to match their respective times at which data was recorded in a new excel sheet according to the type of photovoltaic

technology. Subsequently, this was repeated for all months of the various years. The monthly temperature average was computed for all the months. With the help of a simple MATLAB program, the monthly averages were extracted and plotted against time to obtain the plots of the daily temperature profiles.

II.2. Generating Thermal Cycles

To obtain thermal cycles, six data points per cycle were to be selected: the first point being the first temperature to be recorded in a given day, the second point being the temperature at the end of the first cold dwell, the 3rd point being the temperature at the end of the ramp up or the beginning of the dwell, the 4th point being the temperature at the beginning of the ramp down or the end of the dwell, 5th being the temperature at the end of the ramp down and the 6th point being the temperature at the end of the second cold dwell. Figure 2 demonstrates a labeled thermal cycle and the 6 points selected for simulation. In order to obtain these points, the ramp rate/rate of change from one point to another was computed for all months of the given years. The calculated ramp rates in conjunction with graphical linear fitting were used to identify these points which signify the turning points in the daily temperature cycles. The temperature and time at these points were noted and used to plot a graph with the help of a simple MATLAB program.

The Dwell times were also obtained as follows.

The hot dwell time was given by:

$$T_{hot\ dwell} = T_4 - T_3 \tag{1}$$

The first cold dwell was given by:

$$T_{1st\ cold\ dwell} = T_2 - T_1 \tag{2}$$

The second cold dwell was given by:

$$T_{2nd\ cold\ dwell} = T_6 - T_5 \tag{3}$$

Where T₁, T₂, T₃, T₄, T₅, and T₆ are the respective times obtained from the thermal cycle.

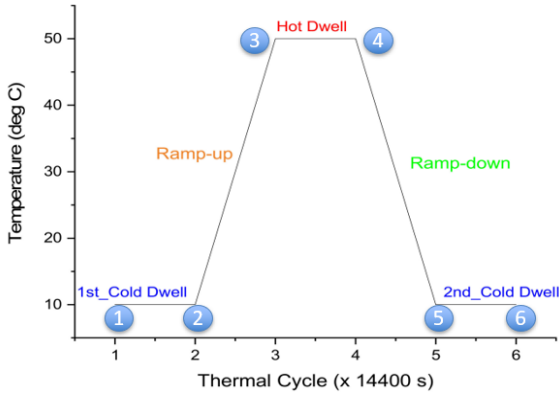


Figure 2. Sample of a daily thermal cycle[17].

III. Results and Discussions

The rig setup transmits data recorded at the 5-minute interval and stored on a server from March 2012 to May 2015. The study and data analysis is limited to the year 2014 and the technologies included are monocrystalline silicon, polycrystalline silicon, CIGS, amorphous silicon, and HIT solar modules. This section presents and discusses the results obtained from data analysis for the generation of temperature cycle profiles for the five technologies in the year 2014.

III.1. Modeling procedure

The 288 data points obtained from the test rig were used to plot the monthly average of the daily temperatures against time to generate the temperature cycles for the various technologies of the various years. Table 2 summarizes the statistics of the data obtained from the daily temperature of the various technologies in the year 2014. CIGS recorded the highest maximum temperature of 77.1 °C while polycrystalline silicon recorded the least minimum of 15.7 °C. The maximum mean temperature of 35.4 °C was recorded in CIGS and the lowest mean temperature of 30.9 °C was recorded in polycrystalline.

Table 2. Data summary for all solar module technologies in the year 2014.

	Mon crystalline	Polycrystalline	HIT	CIGS	Amorphous
Mean(°C)	32.3	30.9	31.4	35.4	31.3
Maximum (°C)	66.0	62.9	71.1	77.1	73.8
Minimum (°C)	16.7	15.7	16.6	17.7	16.4
Range (°C)	49.3	47.2	54.5	59.4	57.4
Standard deviation	9.55	8.71	8.71	11.66	8.81
Skewness	0.79	0.82	0.77	0.81	0.78

Figure 3 shows the daily temperature profiles for the year 2014 for all technologies.

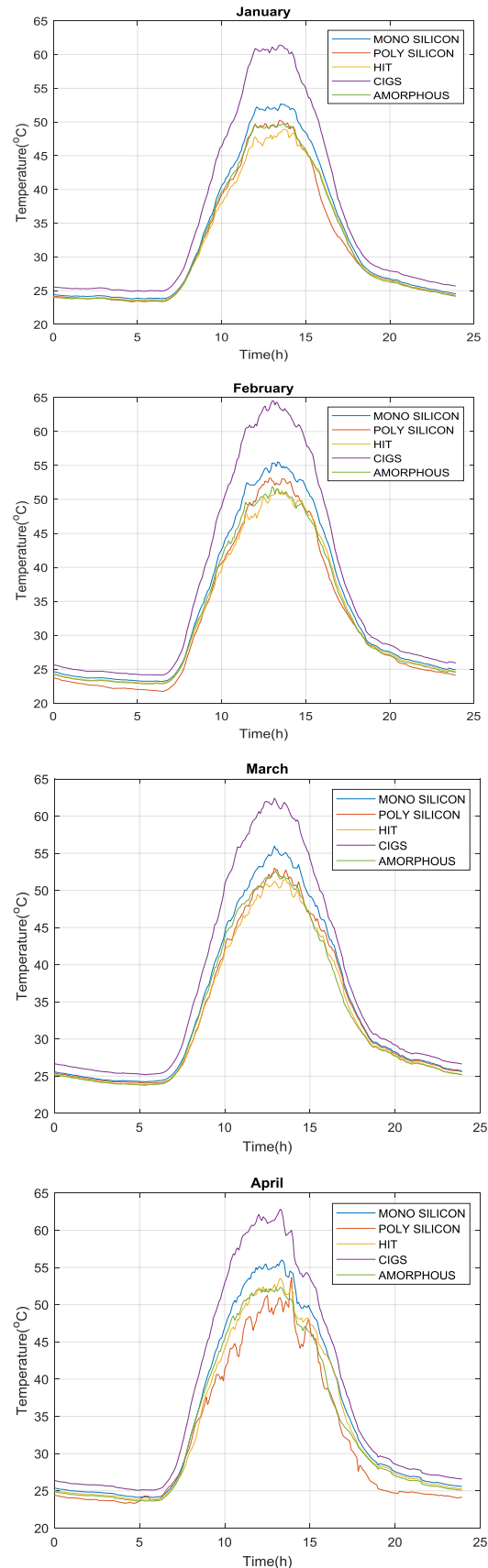


Figure 3(a). Monthly averaged Daily Temperature profiles for January 2014 to April 2014.

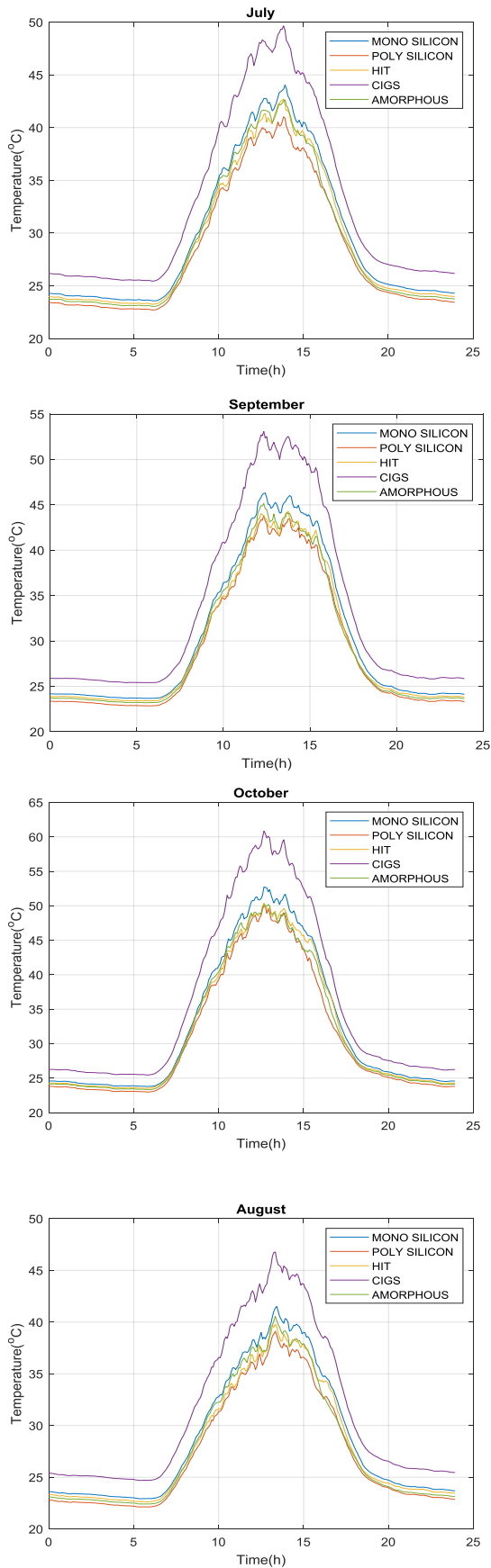


Figure 3(b). Monthly averaged Daily Temperature profiles for May 2014 to October 2014.

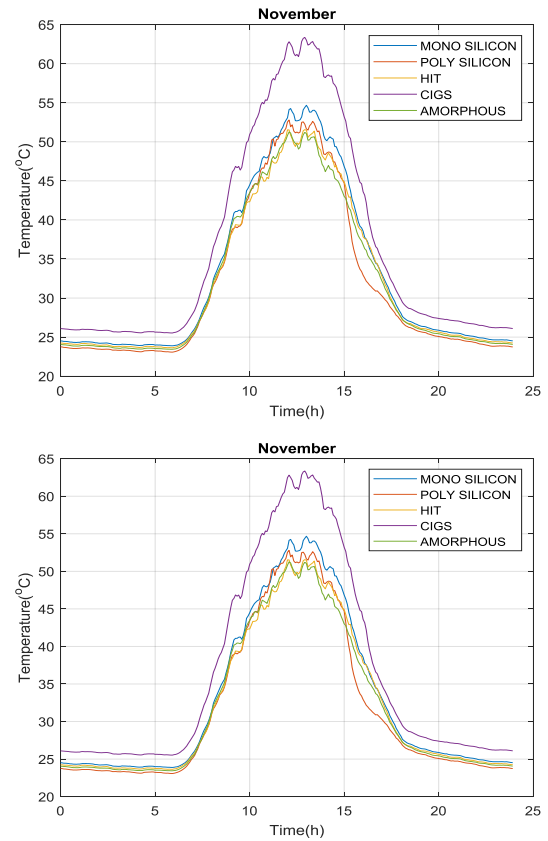


Figure 3(c). Monthly averaged Daily Temperature profiles for November 2014 to December 2014.

High temperatures contribute significantly to reducing the life of a solar module. It results in high stress formed in the solar module due to different coefficients of thermal expansion of module materials which eventually leads to failure. This means that solar modules with higher temperatures are expected to have shorter life [18].

The variation in the difference in coefficient of thermal expansion among the various technologies, along with other material properties may be the reason for different temperature readings in the various technologies despite being installed in the same geographical location under the same solar radiation. The method of manufacturing could also be a contributing factor.

III.2. Temperature Gradient

The change in temperature between the high temperatures in the day and low temperatures at night is referred to as the temperature gradient. It was obtained by identifying the highest and lowest temperatures observed in a given month and finding the difference between them. Hence the temperature gradient is given by

$$\Delta T = T_{MAX} - T_{MIN} \quad (4)$$

Table 3 shows a summary of the frequency of occurrence for temperature gradient expressed in percentage of occurrence for the various technologies for the year 2014. It can be observed that the monocrystalline silicon and the HIT solar module had their temperature gradients within the range of 35 °C -to 49.99 °C and CIGS solar module had temperature gradients within the range of 40 °C -to 59.99 °C. The polycrystalline recorded temperature gradients within the range of 25 °C -to 44.99 °C which was slightly similar in the amorphous silicon solar module which also recorded some temperature gradient occurrence in the range of 55 °C -to 59.99 °C. All the technologies with exception of CIGS recorded the most temperature gradients in the limits of 40 °C -49.99 °C. CIGS recorded the most temperature gradients in the limits of 50°C -to 54.99°C which shows it recorded the highest temperature gradients amongst the other solar modules. Figure 4 shows a frequency distribution of the daily temperature gradients obtained in the year 2014 for all the technologies.

Table 3. Summary of frequency of occurrence of temperature gradient distribution for the year 2014 for all technologies.

FREQUENCY of OCCURANCE					
	Monocrystalline	Polycrystalline	HIT	CIGS	Amorphous
25.00-29.99	-	8.33	-	-	-
30.00-34.99	-	8.33	-	-	8.33
35.00-39.99	16.7	33.3	33.3	-	33.3
40.00-44.99	75	50	58.3	8.33	50
45.00-49.99	8.33	-	8.33	8.33	-
50.00-54.99	-	-	-	75	8.33
55.00-59.99	-	-	-	8.33	-

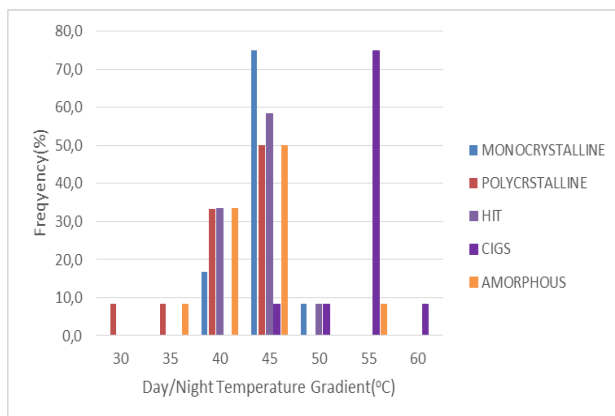


Figure 4. Frequency distribution of the monthly average of daily temperature gradients for various technology module temperatures in the year 2014.

Table 4 shows the mean temperature gradients of all the various technologies in the year 2014. The highest temperature gradient was observed at 51.8 °C in CIGS and the least at 38.4 °C was observed in polycrystalline silicon.

Table 4. Mean temperature gradients of the various technologies in the year 2014.

Year	Monocrystalline (°C)	Polycrystalline (°C)	HIT (°C)	CIGS (°C)	Amorphous (°C)
2014	42.6	38.4	41.1	51.8	40.8

III.3. 3.3 Thermal Cycles

The thermal cycles were obtained using the average ramp rates in conjunction with linear curve fitting of the daily temperature profiles. The six points were obtained and their respective times and temperatures were used to plot the thermal cycles. For example, in January 2014 shown in Figure 3(a), it was observed that the average ramp rate between point 1 and point 84 was a very small negative decimal approaching zero. This number authenticated the graphical nature of the first cold dwell, which is characterized by a horizontal line. Beyond point 84, it was observed that ramp rates began to increase significantly till it reached point 146. The average ramp rate was a significant positive value which implied a very steep upward slope, equal to that of a ramp-up. Between point 146 and point 172 was a dwell. After point 172, the ramp rate was seen to be a significant negative value which implied a steep downward slope, equal to that of a ramp down. After point 227 the average ramp rate was seen to be a small negative value hence the slope became less downward steep up to point 288, which was equal to that of the second cold dwell. Hence these points were translated into time steps for the 6 data points required for the simulations; 0:00 GMT, 6:55 GMT, 12:05 GMT, 14:15 GMT, 18:50 GMT, and 23:55 GMT respectively. The temperatures recorded at these times were also noted. The temperature at point 3 was equated to point 4 to emulate the dwell. This procedure was repeated for all the months and years for the various technologies. The times and temperatures were extracted with help of a MATLAB program and used to plot a yearly module temperature cycle for the various photovoltaic technologies.

Figure 5 shows the thermal cycles of the various technologies for the year 2014. The maximum temperatures slightly increased from January to March, reduced till August, and then increased till December. The trends of the thermal cycles for the various technologies are a result of the weather changes associated with the climate seasons in Ghana, namely the dry season and the rainy season. The dry season occurs from November to March, which explains the observation of high peak temperatures during these months, in the thermal cycles. The rainy season, on the other hand, occurs from April to September/November

which explains the low peak temperatures recorded during these months in the thermal cycles [21].

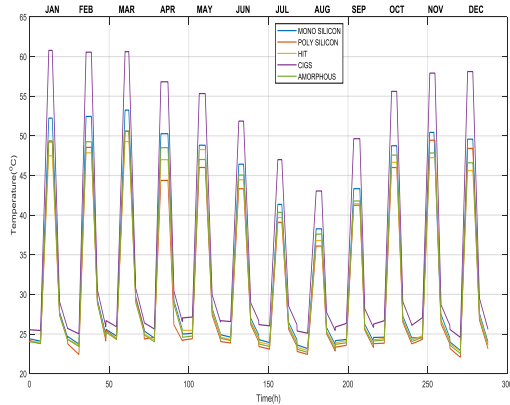


Figure 5. Thermal cycles for the year 2014

III.4. Ramp Rate

The ramp-up rate signifies the rate at which temperature rises at a significant amount from the 1st cold dwell to the dwell. It can then be referred to as the heating rate. The ramp-down rate signifies the rate at which temperature reduces at a significant rate from the dwell to the 2nd cold dwell hence can also be referred to as the cooling rate. Table 5 shows a summary of the ramp rates in the year 2014 for all technologies. The highest mean heating rate of 5.95 °C /h was found in CIGS solar module with a maximum heating rate of 7.76 °C /h and the least heating rate of 4.31 was observed in HIT solar module with a maximum heating rate of 5.39°C/h. The highest mean cooling rate of 6.09 °C /h was observed in CIGS with a maximum cooling rate was 7.67 °C /h and the least mean cooling rate of 4.45°C/h with a maximum cooling rate of 5.29 °C /h was observed in amorphous silicon solar module.

The results on the ramp rates are graphically presented in Figure 6 which shows the distribution of the mean and maximum for the ramp-up and ramp-down rates in the year 2014 for the various technologies

Table 5. Ramp Rates for the various technologies in the year 2014.

Ramp Rates	Monocrystalline	Polycrystalline	HIT	CIGS	Amorphous
Mean Ramp Up Rate(°C/h)	4.94	4.48	4.31	5.95	4.57
Maximum Ramp Up Rate(°C/h)	6.30	5.84	5.39	7.76	5.74
Mean Ramp Down Rate(°C/h)	5.04	4.55	4.58	6.09	4.45
Maximum Ramp Down Rate (°C/h)	6.12	5.76	5.37	7.67	5.29

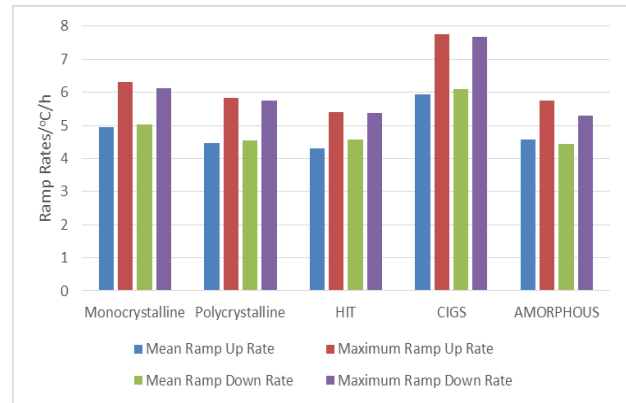


Figure 6. Distribution of the mean and maximum ramp rates in the year 2014 for the various technologies.

It was observed that ramp rates for CIGS solar modules were consistently the highest among all the other solar modules. This was then followed by monocrystalline. HIT, polycrystalline silicon, and amorphous silicon modules were often in varying positions. The mean ramp rates obtained in this study were slightly lower than the ramp rates observed in a similar study [15].

Observing the ramp-up and ramp-down rates shows that their respective values relate closely to each other which is similar to the IEC thermal cycle with ramp-up and ramp-down rates both at 100C/h [8]. This means that the rate at which temperatures rise to the peak of the day is the same rate from after the peak to the night. The study showed that faster ramp rates led to more damage in the solder joint than slower ramp rates [22]. Another study expected that the solar module with the highest ramp rates should have the shortest life [20].

III.5. 3.5 Temperature Dwell Times

In theory, the temperature dwell time refers to the time in the temperature cycle profile when there is no increase in temperature hence zero ramp rates. In practical application, the hot dwell occurs at the time when there is a significant decrease in the ramp-up/heating rate. The 1st and 2nd dwell occur at the time when there are minimal ramp rates before ramp-up starts and after ramp-down ends respectively. The dwell times were obtained using equations (1) (2) and (3) mentioned in section 2.

With respect to all the solar module technologies (monocrystalline, polycrystalline, amorphous silicon, CIGS, and HIT), it was observed that dwell times were the same each month. However, across the months of the year 2014, different hot and cold dwell times were recorded. Figure 7 shows the mean monthly distribution for the hot dwell, 1st, and 2nd cold dwell times in the year 2014 for all the technologies. The mean hot dwell time was observed to be 190 minutes with a maximum of 265

minutes in April and a minimum of 130 minutes in January. The mean 1st and 2nd cold dwell times were 398 and 320 minutes respectively. The maximum for the 1st and 2nd cold dwell times were 420 and 350 minutes respectively, with both recorded in February and the minimum for the 1st and 2nd cold dwell times were 375 and 300 minutes respectively, with both recorded in June. The trend of dwell times correlates with the trend of the thermal cycles and climate in Ghana [21]. This implies that dwell times are longer during dry seasons and shorter in the rainy seasons.

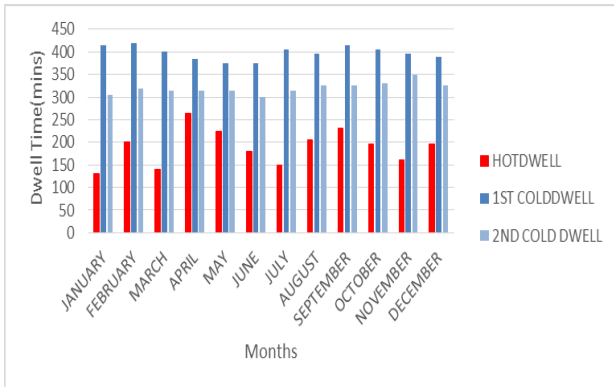


Figure 7. Monthly mean distribution of hot dwell, 1st and 2nd cold dwell times for the year 2014 for all technologies.

The mean hot dwell and cold dwell times in this study were about 3 hours and 6 hours respectively which are closely related to dwell times obtained in a similar study [15]. Longer dwell times contributed significantly to reducing the fatigue life of solder joints by causing more creep [22].

Although dwell times for the various technologies are the same, dwells were seen to occur at different temperatures.

Table 6 shows the mean hot dwell temperatures (HDT) and mean cold dwell temperatures (CDT) in the year 2014 for the various technologies. The highest mean hot dwell temperature was observed in CIGS with the highest of them being 54.78 °C. The lowest hot dwell temperature of 45.15 °C was seen in HIT. The highest cold dwell temperature of 26.12 °C was seen in CIGS with the lowest cold dwell temperature of 23.88 °C seen in polycrystalline.

Table 6. Summary of Mean Hot Dwell Temperatures (HDT) and Mean Cold Dwell Temperatures (CDT) for the various technologies in the year 2014.

Monocrystalline		Polycrystalline		HIT		CIGS		Amorphous	
Mean	Mean	Mean	Mean	Mean	Mean	Mean	Mean	Mean	Mean
HDT/°C	CDT/°C	HDT/°C	CDT/°C	HDT/°C	CDT/°C	HDT/°C	CDT/°C	HDT/°C	CDT/°C
47.93	24.63	45.20	23.88	45.15	24.36	54.78	26.12	45.97	24.17

III.6. Comparison between IEC 61215 and 2014 thermal cycle

The thermal cycles of the various technologies were compared with IEC 61215 thermal cycle and the percentage differences for the parameters evaluated above were obtained.

Table 7 shows a summary of the percentage difference of parameters between the thermal cycles of the various technologies in the year 2014 and the IEC 61215 thermal cycle. The IEC 61215 is characterized by high ramp rates, short dwell times, and a high-temperature gradient. It is performed over a short cycle time (10200s). On the other hand, the thermal cycles of the various technologies had low ramp rates, long dwell times, low-temperature gradients, and longer cycle times (86400s).

III.6.1. Ramp Rates

The percentage difference in ramp-up and ramp-down rates between the monocrystalline silicon and IEC 61215 was -95.1% and -95.0% respectively. The ramp-up and ramp-down rates of polycrystalline silicon compared to the IEC 61215 were both -95.5%. The ramp-up and ramp-down rates of HIT compared to the IEC 61215 were -95.7% and -95.4% respectively. The ramp-up and ramp-down rates of CIGS compared to the IEC 61215 were -94.1% and 93.9% respectively. The ramp-up and ramp-down rates of amorphous compared to the IEC 61215 were -95.4% and 95.6% respectively. The highest percentage difference was seen in HIT while the lowest was seen in CIGS. This shows that the ramp rates of the IEC 61215 were extremely larger than that of the various technologies with the CIGS having the highest ramp rates among the other technologies.

III.6.2 Dwell Times

Dwell times were the same across the various technologies. Compared with the IEC 61215, the hot dwell and cold dwell from all the technologies had a difference of 1796% and 3489.5% respectively. This shows that the dwell times of the various technologies were significantly higher compared to IEC 61215. This is because the nature of the weathering conditions is such that daytime temperatures remain fairly constant for about 3 hours nearing the highest day temperatures and nighttime temperatures remain fairly constant for about 7 hours nearing the lowest night temperatures.

III.6.3 Maximum, Minimum, and Temperature Gradient

The maximum, minimum, and temperature gradients of the mono-crystalline silicon thermal cycle compared to that of the IEC 61215 had percentage differences of -43.6%, -161.6%, -81.4% respectively. The maximum,

minimum, and temperature gradients of the polycrystalline crystalline silicon thermal cycle compared to that of the IEC 61215 had percentage differences of -46.8%, -159.7%, -82.9% respectively. The maximum, minimum, and temperature gradients of the HIT thermal cycle compared to that of the IEC 61215 had percentage differences of 46.9%, -160.9%, and -83.4% respectively. The maximum, minimum, and temperature gradients of the CIGS thermal cycle compared to that of the IEC 61215 had percentage differences of -35.6%, -165.3%, and -77.1% respectively. The maximum, minimum, and temperature gradients of the mono-crystalline silicon thermal cycle compared to that of the IEC 61215 had percentage differences of -45.9%, -160.4%, and -82.6% respectively. The highest difference in maximum temperature was observed in polycrystalline while the lowest difference was seen in CIGS as shown in Table 7. With minimum temperature, the highest difference was seen in CIGS with the lowest difference in polycrystalline. The greatest difference in temperature gradient was seen in HIT with the least difference seen in CIGS. This shows that the temperatures of the various technologies were significantly lower than that of the IEC 61215.

Table 7. Summary of the percentage difference between thermal cycles of the various technologies in the year 2014 and the IEC 61215 thermal cycle.

Thermal Cycle	Ramp Rates °C/h		Dwell Times /min		Maximum Temperature /°C	Minimum Temperature /°C	Temperature Gradient /°C
	Ramp UP	Ramp Down	Hot	Cold			
IEC 61215	100.0	100.0	10.0	10.0	85.0	-40.0	125.0
Monocrystalline	4.9	5.0	189.6	359.0	47.9	24.6	23.3
% Difference%	-95.1%	-95.0%	1796.0%	3489.5%	-43.6%	-161.6%	-81.4%
Polycrystalline	4.5	4.6	189.6	359.0	45.2	23.9	21.3
% Difference%	-95.5%	-95.5%	1796.0%	3489.5%	-46.8%	-159.7%	-82.9%
HIT	4.3	4.6	189.6	359.0	45.2	24.4	20.8
% Difference%	-95.7%	-95.4%	1796.0%	3489.5%	-46.9%	-160.9%	-83.4%
CIGS	6.0	6.1	189.6	359.0	54.8	26.1	28.7
% Difference%	-94.1%	-93.9%	1796.0%	3489.5%	-35.6%	-165.3%	-77.1%
Amorphous	4.6	4.5	189.6	359.0	46.0	24.2	21.8
% Difference%	-95.4%	-95.6%	1796.0%	3489.5%	-45.9%	-160.4%	-82.6%

IV. Conclusion and Recommendation

In this study, outdoor weathering data from a rig setup in Kumasi was used to generate thermal cycles for 5 different technologies namely Monocrystalline silicon, Polycrystalline silicon, Heterojunction with an intrinsic thin layer (HIT), Copper Indium Gallium Selenide (CIGS), and Amorphous silicon solar modules in the year 2014. Key parameters which included maximum, and

minimum temperatures, ramp rates, and hot and cold dwell times were obtained.

The thermal cycles in the year 2014 had the most amount of data and hence were the most suitable to be used for further studies on thermomechanical reliability. The maximum, minimum, and ramp rates for the various technologies in the year 2014 were 47.9 °C, 24.6 °C, 4.95 °C/h for Monocrystalline silicon, 45.2 °C, 23.9 °C, 4.55 °C/h for Polycrystalline silicon, 45.2 °C, 24.4 °C, 4.45 °C/h for HIT, 54.8 °C, 26.1 °C, 6.05 °C/h for CIGS and 46.0 °C, 24.2 °C, 4.55 °C/h for Amorphous silicon solar modules respectively. Parameters in CIGS were constantly the highest, followed by monocrystalline silicon and then polycrystalline silicon, amorphous silicon, and HIT which were closely related. Hot dwell and cold times were 189 minutes and 359 minutes respectively for all the technologies. A comparison between the thermal cycles of the various technologies and the IEC 61215 thermal cycle showed massive differences. The percentage differences of the various technologies were in the ranges of -35.6% to -46.9% for maximum temperatures, -35.6% to -46.9% for minimum temperatures, -159.7% to -165.3% for minimum temperatures, -94% to -95.55% for ramp rates, and 1796% and 3489.5% for the hot and cold dwell times.

In light of the findings obtained from this research, the author recommends that the thermal cycling for the various technologies under outdoor weathering in Kumasi may be used to carry out reliability testing to assess thermomechanical fatigue in the solder joints of the solar modules. This is necessary to evaluate the damage exposed to the solder joints by thermal stress and provide knowledge on the expected life. Thermal cycling is location-dependent hence similar research may be repeated to obtain thermal cycles in various test sites in Ghana.

Acknowledgment

The US National Academy of Sciences provided funding for the PRESSA project Sub-Grant no. 2000004829, which the authors gratefully acknowledge. The Arizona State University Photovoltaic Reliability Laboratory's Dr. Mani and Sai Tatapudi's technical assistance is greatly appreciated by the authors. The authors also acknowledge the Norwegian Program for Capacity Development in Higher Education and Research for Development in the Fields of Energy and Petroleum (EnPE) for the support provided.

Declaration

- The authors declare that they have no known financial or non-financial competing interests in any material discussed in this paper.
- The authors declare that this article has not been published before and is not in the process of being published in any other journal.
- The authors confirmed that the paper was free of plagiarism.

References

- [1] M. Aghaei et al., "Review of degradation and failure phenomena in photovoltaic modules," *Renewable and Sustainable Energy Reviews*, vol. 159, 2022, pp. 112160, doi: 10.1016/j.rser.2022.112160.
- [2] V. Devabhaktuni et al., "Solar energy: Trends enabling technologies," *Renewable and Sustainable Energy Reviews*, vol. 19, 2013, pp. 555–564, doi: 10.1016/j.rser.2012.11.024.
- [3] A. Smets, K. Jaeger, O. Isabella, R. Van Swaaij, M. Zeman, "Fundamentals, Technology and Systems, Solar energy," vol. 1. uit cambridge ltd, 2016.
- [4] M. T. Zarmai, N. N. Ekere, C. F. Oduoza, E. H. Amalu, "Optimization of thermo-mechanical reliability of solder joints in crystalline silicon solar cell assembly," *Microelectronics Reliability*, 2015, pp. 117-125. doi:10.1016/j.microrel.2015.12.031
- [5] S. Chaparala, J. M. Pitarresi, and M. Meilunas, "Effect of Dwell Times and Ramp Rates on the Thermal Cycling Reliability of Pb-free Wafer- Level Chip Scale Packages-Experiments and Modeling.," Conference: ASME International Mechanical Engineering Congress and Exposition, 2006, DOI: 10.1115/IMECE2006-13376
- [6] E. H. Amalu, D. J. Hughes, F. Nabhani, J. Winter, "Thermo-mechanical deformation degradation of crystalline silicon photovoltaic (c-Si PV) module in operation," *Eng. Fail. Anal.*, vol. 84, no. 2018, pp. 229–246, doi: 10.1016/j.engfailanal.2017.11.009.
- [7] D. Ghaderi, M. Pourmahdavi, "Combination of thermal cycling and vibration loading effects on the fatigue life of solder joints in a power module," *Journal of Materials: Design and Applications*, vol. 233, 2018, doi: 10.1177/1464420718780525.
- [8] C. B. Jones, B. Hamzavy, W. B. Hobbs, C. Libby, O. Lavrova, "IEC 61215 Qualification Tests vs Outdoor Performance using Module Level In Situ I-V Curve Tracing Devices," 7th World Conference on Photovoltaic Energy Conversion, 2018, DOI: 10.1109/PVSC.2018.8548222
- [9] G. Cuddalorepatta, A. Dasguptal, S. Sealing, J. Moyer, T. Tolliver, J. Loman, "durability of pb-free solder connection between copper interconnect wire and crystalltne silicon solar cells," 2006, DOI: 10.1109/ITHERM.2006.1645486
- [10] S. P. Aly, S. Ahzi, N. Barth, A. Abdallah, "Numerical analysis of the reliability of photovoltaic modules based on the fatigue life of the copper interconnects," *Solar Energy*, vol. 212, no. April, 2020, pp. 152–168, doi: 10.1016/j.solener.2020.10.021.
- [11] S. M. Shamim, M. B. Science, S. Islam, F. Huq, "Design , performance analysis and efficiency optimization of copper indium gallium selenide (cigs) solar cell," *European Scientific Journal*, vol.11, No.6, 2015.
- [12] L. M. Fraas, "The Dream of Thin Film PV," in *Low-Cost Solar Electric Power*, Springer International Publishing, 2014, pp. 73–79.
- [13] F. K. A. Nyarko, G. Takyi, E. H. Amalu, M. S. Adaramola, "Generating temperature cycle profile from in-situ climatic condition for accurate prediction of thermo-mechanical degradation of c-Si photovoltaic module," *Engineering Science and Technology, an International Journal*, 2018, doi: 10.1016/j.jestch.2018.12.007
- [14] U. Eitner, S. Kajari-schr, K. Marc, and H. Altenbach, "Thermal Stress and Strain of Solar Cells in Photovoltaic Modules," Part of the *Advanced Structured Materials* book series, 2011, pp. 453–468.
- [15] N. Park, J. Jeong, C. Han, "Microelectronics Reliability Estimation of the degradation rate of thermal-crystalline silicon photovoltaic module under thermal cycling stress," *Microelectron. Reliab*, *Microelectronics Reliability*, vol . 54 , 2014, pp. 1562–1566, doi:10.1016/j.microrel.2014.03.021
- [16] N. Amin, C. Wen, K. Sopian, "A practical field study of various solar cells on their performance in Malaysia," *Renew. Energy*, vol. 34, no. 8, 2009, pp. 1939–1946, doi: 10.1016/j.renene.2008.12.005.
- [17] F. K. Nyarko, Afriyie, G. Takyi, A. A. Agyemang, C. S. K. Kofi, "Crystalline Silicon (c-Si) Solar Cell interconnect damage prediction function based on effect of temperature ramps and dwells on creep damage under field thermal cycling," *Crystals and Thin Films* , 2021, vol. 633 , <https://doi.org/10.3390/cryst11060633>
- [18] O. M. Al-hababbeh, B. A. Al-hrout, E. A. Al-hiary, S. A. Al-fraihat, "Durability Prediction of Thin-film PV Modules Durability Prediction of Thin-film PV Modules," *Int'l J. Eng. Simulation with Indust. Applications (IJES)*, vol. 15, 2014, pp.13-21.
- [19] W. Herrmann, N. Bogdanski, F. Reil, K.-A. Weiss, M. Assmus, M. Heck, "PV module degradation caused by thermomechanical stress: real," *Reliability of Photovoltaic Cells, Modules, Components, and Systems III*. doi:10.1117/12.859809
- [20] S. C. Chaparala et al., "Effect of Geometry and Temperature Cycle on the Reliability of WLCSP Solder Joints," *IEEE Transactions on Components and Packaging Technologies*, 2005, pp. 441–448.
- [21] K. Owusu, P. R. Waylen, "The changing rainy season

- climatology of mid-Ghana,” *Theoretical and Applied Climatology*, vol 112, 2012, pp. 419–430, doi:10.1007/s00704-012-0736-5
- [22] X. Fan, G. Raiser, V. S. Vasudevan, “Effects of dwell time and ramp rate on lead-free solder joints in fcbga packages,” *Proceedings Electronic Components and Technology*, 2005, DOI: 10.1109/ECTC.2005